



HAL
open science

Tunable mid IR plasmon in GZO nanocrystals

M. Hamza, Jean-Marie Bluet, Karine Masenelli-Varlot, B. Canut, O. Boisron,
P. Mélinon, B. Masenelli

► **To cite this version:**

M. Hamza, Jean-Marie Bluet, Karine Masenelli-Varlot, B. Canut, O. Boisron, et al.. Tunable mid IR plasmon in GZO nanocrystals. *Nanoscale*, 2015, 7 (28), pp.12030-12037. 10.1039/C5NR03378K . hal-01965002

HAL Id: hal-01965002

<https://hal.science/hal-01965002>

Submitted on 29 Mar 2021

HAL is a multi-disciplinary open access archive for the deposit and dissemination of scientific research documents, whether they are published or not. The documents may come from teaching and research institutions in France or abroad, or from public or private research centers.

L'archive ouverte pluridisciplinaire **HAL**, est destinée au dépôt et à la diffusion de documents scientifiques de niveau recherche, publiés ou non, émanant des établissements d'enseignement et de recherche français ou étrangers, des laboratoires publics ou privés.

Tunable mid IR plasmon in Gallium doped ZnO nanocrystals

M.K. Hamza¹, J-M. Bluet¹, K. Masenelli-Varlot², B. Canut¹, O. Boisron³, P. Melinon³, B. Masenelli^{1,*}

¹ Institut des Nanotechnologies de Lyon, INSA-Lyon, UMR CNRS 5270, Université de Lyon, 7 avenue Jean Capelle, 69621 Villeurbanne Cedex, France

² Université de Lyon, INSA-Lyon, MATEIS UMR CNRS 5510, 7 avenue Jean Capelle, 69621 Villeurbanne Cedex, France

³ Institut Lumière Matière, Université Lyon 1, UMR CNRS 5306, Université de Lyon, 69622 Villeurbanne cedex, France

Abstract

Degenerate metal oxide nanoparticles are promising systems to expand the significant achievements of plasmonics into the infrared (IR) range. Among the possible candidates, Ga-doped ZnO nanocrystals are particularly suited for mid IR, considering their wide range of possible doping level and thus of plasmon tuning. In the present work, we report on the tunable mid IR plasmon induced in degenerate Ga-doped ZnO nanocrystals. The nanocrystals are produced by a plasma expansion and exhibit unprotected surfaces. Tuning the Ga concentration allows tuning the localized surface plasmon resonance. Moreover, the plasmon resonance is characterized by a large damping. By comparing the plasmon of nanocrystals assemblies to that of nanoparticles dispersed in an alumina matrix, we investigate the possible origins of such damping. We demonstrate that it partially results from the self-organization of the naked particles but also from intrinsic inhomogeneity of dopants.

*Corresponding author : bruno.masenelli@insa-lyon.fr

Introduction

After having been extensively studied as TCO (transparent conductive oxide), highly doped (degenerate) metal oxide semiconductors are now being considered as a promising platform for the expansion of plasmonics in the IR [1, 2]. The possibility to achieve plasmons in the near IR (NIR) in Al or Ga doped ZnO thin films, as well as in ITO (indium tin oxide) ones has been demonstrated [3,4,5] and even harvested to build metamaterials [6].[7]. Whilst plasmonic materials in the NIR ranges have remarkably advanced, the exploitation of low-cost and reliable MIR materials remains yet a challenge. The pursuance of MIR plasmonics would add a substantial value to technological applications such as chemical sensing, bio-diagnostics, thermography, emitters, and near-field imaging. In particular, the mid IR (MIR) range is the domain where many molecules or chemical species exhibit strong optical resonances due to vibrational modes. This feature is the motivation of FTIR (Fourier Transform InfraRed) spectroscopy. In order to improve chemical sensing through IR spectroscopy, it is highly desirable to reproduce in the IR range the improvements of chemical sensing achieved in the visible range thanks to the use of plasmons in noble metal particles. For this purpose, designing nanoparticles that can sustain a MIR plasmon is of prime importance. This can be done either dynamically by inducing an electron gas in the conduction band of the particles using a pulsed high power laser [8,9,10] or by chemically doping the particles. The former strategy is interesting for high speed switches while the latter is better-suited to steady-state chemical sensing. Several recent studies have demonstrated that the chemical doping is possible in oxide nanoparticles made of ITO, Al-doped ZnO (AZO), Ga-doped ZnO (GZO), or Sn-doped ZnO, ICO (indium doped Cadmium Oxide) and even WO_3 [11, 12, 13, 14, 15] as well as in chalcogenide nanocrystals [16, 17, 18]. The major interest with degenerate semiconductors is the ability to tune the plasmon resonance through the control of the density of free charge carriers. Contrary to noble metals, it is possible to tune the plasmon resonance wavelength from about $1 \mu\text{m}$ to $5 \mu\text{m}$ [12] by controlling the carrier density over one order of magnitude (from a few 10^{19} cm^{-3} to more than 10^{21} cm^{-3}). Expanding this

range towards higher concentrations is a real challenge. Specifically, whatever the material, when increasing the carrier concentration and thus the doping fraction, one will face the solubility limit issue. Besides, while IR plasmons have shown to exhibit fewer losses than their noble metal counterparts in thin films [19,20,21], it is not true in nanocrystals. It seems a common feature for assemblies of degenerate metal oxide nanoparticles to exhibit large damping [22]. However this feature is not commented upon and only recently have Milliron and co-workers addressed the issue [23], proposing that the damping is related to the incomplete activation of the doping impurities [24].

In the present work, we report on the physical synthesis of uncapped GZO nanoparticles by a plasma expansion in high vacuum. GZO is an interesting material because of its expected wide range of plasmon tuning (from near IR to mid IR) due to a large doping range. Furthermore, it is based on abundant and thus cheap elements. With free surfaces, the nanoparticles can self-organize. By varying the Ga content within the particles we are able to tune the plasmon wavelength from 3 to 4 μm . We establish that the maximum value of Ga homogeneously incorporated in ZnO nanoparticles resulting from the adiabatic expansion of a plasma lies between 6% and 9%. As expected the plasmon resonance is characterized by a large damping which is correlated to the partial activation of Ga dopants. By dispersing the nanocrystals in an alumina matrix, we synthesize a MIR plasmonic nanocomposite with reduced damping. This demonstrates that beside the heterogeneous distribution of Ga, the self-organization and the related interfaces also control the damping in the assembly.

Methods

Synthesis method

The nanoparticles have been synthesized by the LECBD (low energy cluster beam deposition) technique described in [25]. A plasma is first generated by ablating a target with a high power pulsed

(10 Hz repetition rate) doubled (532 nm) YAG: Nd laser. The target is a pellet made of a mixture of ZnO and Ga₂O₃ (99.999% pure each) microscopic powders sintered and annealed at 800°C for 10h. The plasma is first quenched by a constant flux of gas consisting of 75% He and 25% O₂. The O₂ amount has been chosen to preserve the stoichiometry of the resulting nanocrystals (cf. [25]). The buffer gas induces the stabilization of nucleation embryos (dimers and trimers). On these embryos, atoms from the plasma aggregate according to an accretion process when the plasma expands through a micrometer nozzle while leaving the nucleation chamber at some 20 mbar and reaching the deposition chamber at a few 10⁻⁷ mbar. This important pressure variation (eight orders of magnitude) located over a very small distance (a few microns from the nozzle) leads to an adiabatic expansion of the plasma leading to the hyperquenching of the nanoparticles produced by accretion. The resulting particles form a supersonic jet which is deposited on silicon substrates (see supporting information). Despite their high velocity, the kinetic energy per atom among the particles is lower than the binding energy per atom; this ensures that the particles do not break during deposition. The deposition rate amounts typically to 1 nm/min. This rate can be tuned directly by changing the laser power or its repetition rate. The films resulting from the deposition of the nanoparticles are several hundred of nm thick and look like foam, with a high porosity, estimated to be about 70% from the 3D percolation theory. This is illustrated in scanning electron microscope (SEM) images of the films shown in the supporting information.

Characterization techniques

The structure of the deposited particles has been investigated on the one hand by transmission electron microscopy (TEM) and on the other hand by X-Ray diffraction (XRD). TEM high resolution images were acquired on a JEOL 2010F operating at 200 kV, equipped with a Gatan Orius 100 CCD camera. For the determination of the size distribution of the nanoparticles, isolated nanoparticles were deposited on carbon coated Cu grids (from Ted Pella Inc.). The grids were placed directly in the particle beam for a few seconds to ensure the deposition of isolated particles (the corresponding

equivalent deposited thickness is about 5Å). The contrast due the particle being not so high, the size distribution has been obtained from high resolution TEM images. XRD diffractograms were obtained on a Rigaku Smartlab diffractometer using the Cu K_{α1} radiation ($\lambda = 1.54 \text{ \AA}$). The elemental composition of the particles has been measured at the nanoparticle scale by Energy Dispersive X-ray spectroscopy (EDS) during the TEM analyses (80 mm² SSD detector from Oxford Instrument), at the surface of the nanoparticle assembly by X-ray photoelectron spectroscopy (XPS) using the Al K_α line at 1486.6 eV and at the scale of the whole nanoparticle films by Rutherford Backscattering Spectrometry (RBS) using a ⁴He⁺ ion beam accelerated at 3 MeV delivered by the 4 MV Van de Graaff accelerator of the Nuclear Physics Institute of Lyon (IPNL). The backscattered particles were detected with a 13 keV resolution implanted junction set at an angle of 160° with respect to the beam axis. Furthermore, the presence of plasmon resonance has been probed by FTIR in the reflection mode.

Results

Nanoparticle assembled films

The LECBD technique has already been used to synthesize ZnO nanocrystals [25,26]. The resulting particles are crystallized in the wurtzite structure. In the case of Ga doping at 3%, 6% and 9%, the TEM analysis in the high resolution mode confirms that it is still the case, as illustrated in fig. 1 and in the supporting information. The size distribution of the as-synthesized nanocrystals, measured on a collection of 78, 53 or 48 isolated particles for the 3%, 6% and 9% doped samples, respectively, is visible in Fig. 1b). With a level of confidence of 95%, the mean size of particle distribution could be calculated as $5.6 \pm 0.3 \text{ nm}$, 6.3 ± 1.2 and $6.7 \pm 1.7 \text{ nm}$ for the samples doped at 3%, 6% and 9% respectively.

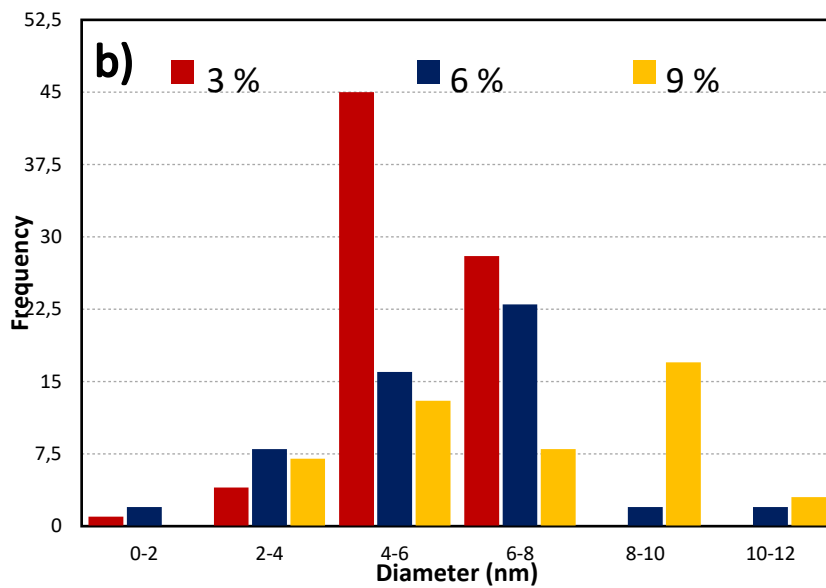
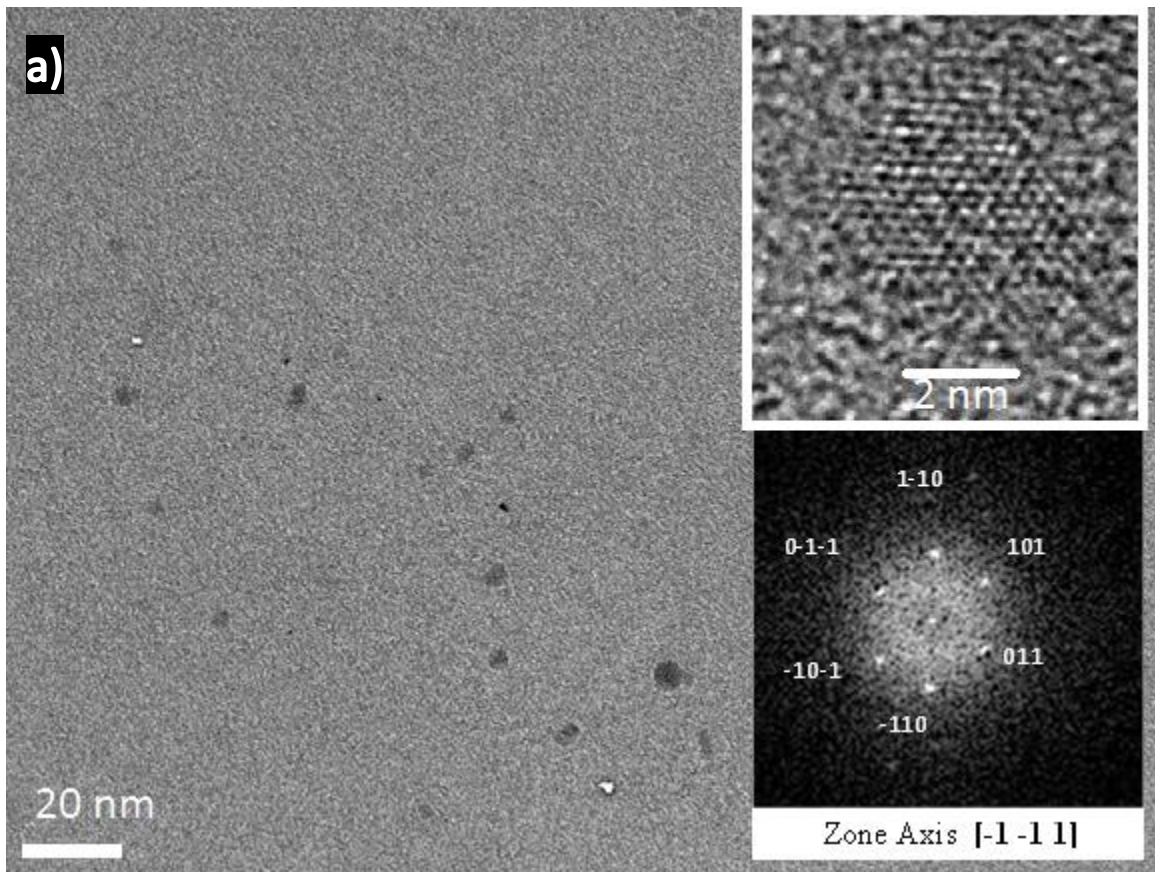


Figure 1: a) low magnification TEM image of isolated GZO nanoparticles. Upper inset: high resolution TEM image of a GZO nanocrystal, doped at 3% with Ga. The lower inset is the FFT of the nanocrystal, confirming the wurtzite structure of the particle. b) size distribution of the as-deposited diluted nanocrystals for the three different Ga concentrations.

The wurtzite structure is confirmed by XRD on the films resulting from the deposition of the nanocrystals (see fig. 2). No other phase, and in particular any phase related to pure Ga or Ga compound, is observed. However, the mean size of the crystalline domains as deduced by Scherrer's equation, assuming perfect crystals without defects, is 18.7 nm, 20.7 nm and 20.4 nm for the 3%, 6% and 9% doped GZO samples respectively. This discrepancy has already been noticed for pure ZnO nanocrystals produced by the LECBD technique [26] as well as by other techniques (see [27] and references therein). It results from the oriented attachment (OA) of the initial uncapped nanocrystals which tend to reduce the energy of the free surface of their facets by epitaxial attachment. Indeed, when the nanoparticles reach the substrate, they conserve a certain kinetic energy. This kinetic energy allows them to rotate a little upon impact on the sample and present their facets to those of other already present nanoparticles. This leads to the sticking of neighboring nanoparticles. Because the facets are uncapped they can arrange so as to minimize the interface energy. This is done when epitaxy is achieved, giving rise to larger single crystal domains. Because the OA is a statistical process, the resulting domains are very likely to be non spherical. OA is a quite general process in systems using nanoparticles as primary building blocks (for a complete review, see [27]). An example of two nanocrystals attached according to this process is given in supplementary information. The result of the OA is thus larger crystalline domains which are not quasi-spherical anymore and with defects at the interfaces because of an imperfect epitaxy. To name a few, we can mention twin boundaries and dislocations. The XRD analysis also provides us with the mean reticular spacing. As expected, since gallium has an ionic radius of 0.62Å and covalent radius of 1.26Å, which are close to those of zinc (0.74 Å and 1.31 Å), the increase in the inter-reticular distance is very small (supplementary information): it increases almost linearly with the Ga fraction and reaches only 0.38% at 9% Ga .

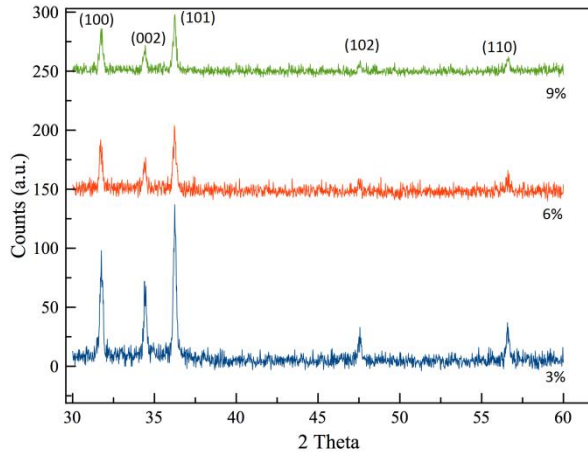


Figure 2: diffractograms of GZO nanocrystal samples with 3%, 6% and 9% Ga content.

Table 1: Ga content (at. % with respect to Zn) of the GZO nanocrystals as deduced from different techniques, EDS (at the particle scale), RBS (at the whole film scale) and XPS (at the scale of the first nanoparticle layer). Mean Ga concentration (deduced from RBS) and free electron density (deduced from Drude's model applied to the plasmon resonance). The ratio n/n_{Ga} indicates the fraction of Ga dopant actually contributing to the plasmon.

Nominal composition	XPS	EDS	RBS	$n_{\text{Ga}}(\text{cm}^{-3})$	$n(\text{cm}^{-3})$	n/n_{Ga}
3%	$2 \pm 1\%$	$4 \pm 2\%$	$3 \pm 1\%$	$3.3 \cdot 10^{20}$	$1.8 \cdot 10^{20}$	0.5
6%	$5 \pm 1\%$	$6 \pm 2\%$	$8 \pm 1\%$	$5.8 \cdot 10^{20}$	$3.5 \cdot 10^{20}$	0.6
9%	$5.4 \pm 1\%$	8 to 45%	$13 \pm 1\%$	$9.7 \cdot 10^{20}$	$4.1 \cdot 10^{20}$	0.4

The chemical compositions of the samples as deduced by EDS, XPS and RBS are summed up in table 1. The RBS technique which probes the films over a large area ($\sim 1 \text{ mm}^2$) and in complete depth gives values which should be considered as reference values to be compared to values from other techniques. The XPS analysis, which probes the same area but on a much smaller depth (of about 10 nm), is in fair accordance with the RBS results and the nominal values for the lowest doping levels

but is drastically different for the larger doping level. Instead of the 9% doping expected, we only measure a Ga content of 5%. This suggests that for the highest doping level the Ga distribution is not homogeneous along the deposition direction. It is likely that as the ablation of the target occurs, the composition of plasma changes either because the target is not homogeneous in depth or because the ablation is a selective process for the highly doped target. When we probe the samples at the scale of individual particles by EDS, the composition is rather constant from particle to particle for the 3% and 6% doped GZO nanocrystals. A variation of $\pm 2\%$ is found. However, for the 9% doped sample, strong variations of the Ga content are evidenced from particle to particle, some exhibiting 8% Ga content while others have 45% of Ga. In accordance with the XPS analysis, we can conclude that the incorporation of Ga is homogeneous for concentrations lower than 9%. This observation is interesting regarding the solubility limit issue. Several scenarios have been evoked regarding the incorporation of impurities in nano-objects [28]. On the one hand, if the synthesis is ruled by thermodynamics, the dopant solubility in nanoparticles should be lower than the bulk one (measured between 0.5% and 1.5% in bulk ZnO [29]), leading to self-purification and dopant segregation at the particle surface. On the other hand, if kinetics rules the synthesis, the solubility limit can be higher in nanoparticles than in the bulk and the location should be homogenous throughout the nanoparticle. In our synthesis technique, the particle growth is obviously ruled by kinetics. However, the Ga content is inhomogeneous from particle to particle and, even if some particles can incorporate an amount of Ga impurities larger than the thermodynamic limit, it is not sure at all whether the Ga atoms are rejected at the surface or not, leading to a kind of self-purification mechanism. Further studies are necessary to investigate this point which is of prime importance to reach the maximum efficient incorporation amount of Ga in ZnO nanoparticles.

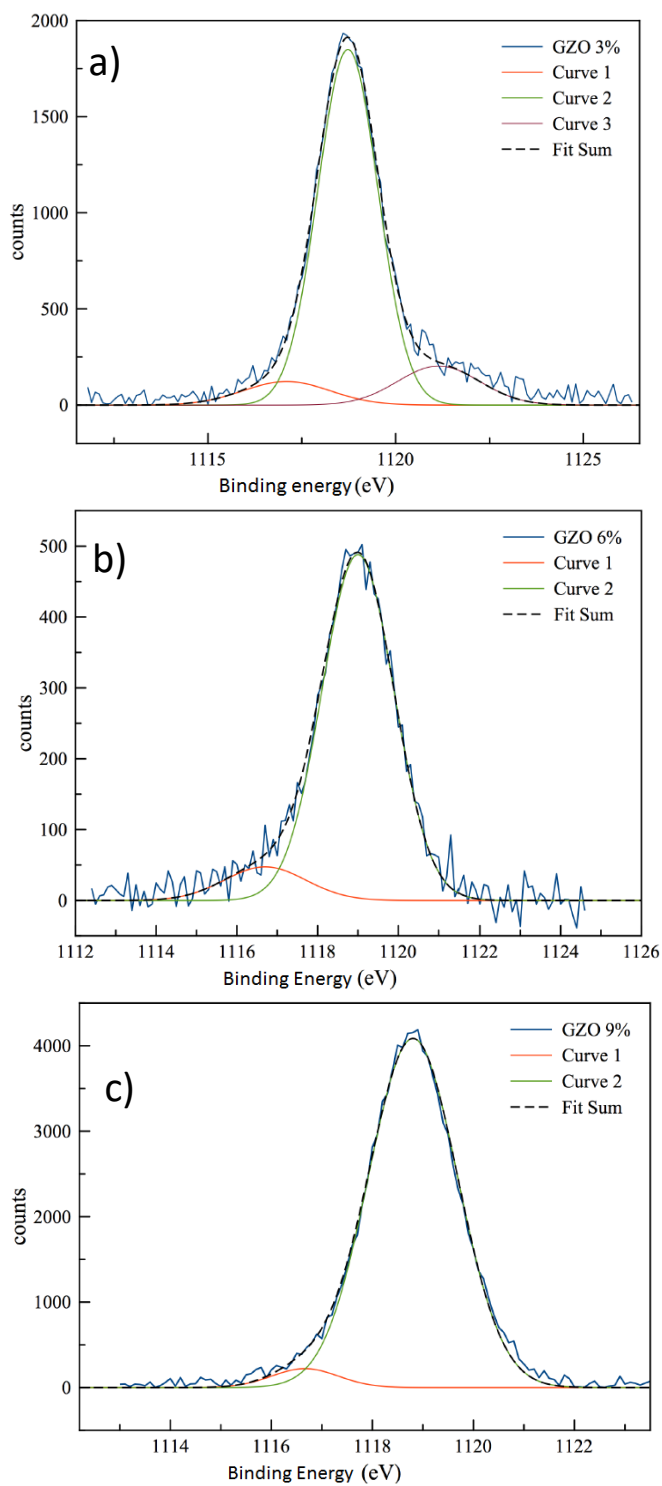


Figure 3: Ga 2p_{3/2} peak for the 3%, 6% and 9% doped GZO nanoparticles (a), b) and c) respectively).

The XPS analysis also provides hints on the local chemical environment of the species in the GZO nanocrystals. In particular, we are interested in the chemical state of Ga dopants. Figure 3 shows the Ga $2p_{3/2}$ peak for the three concentrations of Ga. Each peak can be decomposed into two contributions which are fitted by Gaussian functions. The prominent one, centered at 1118.9 ± 0.2 eV, is attributed to Ga^{3+} ions bound to O [30,31,32]. These ions may be in substitution of Zn^{2+} in the wurtzite ZnO structure. The second one, peaking at 1116.8 ± 0.2 eV, can originate from metallic Ga [31,33]. It is worth noticing that its intensity is about one tenth of the prominent contribution. A third minor contribution is observed only for the 3% doped GZO nanoparticles, peaking at 1121 ± 0.2 eV. This contribution can hardly be assigned to Ga and no hypothesis is proposed yet. A complete detailed analysis of the XPS results is presented in the supplementary information.

The effect of Ga doping on the IR optical properties of the nanocrystal assembled films has been investigated by FTIR reflectance measurements. The results are shown in fig. 4. As compared to pure ZnO nanocrystals, we can observe a reduction of the reflectivity around 2500 cm^{-1} ($4 \mu\text{m}$) for all GZO samples. A broad band can be seen which shifts from $4 \mu\text{m}$ to $3 \mu\text{m}$ as the Ga content increases from 3% to 9%. This shift is in accordance with a plasmonic behavior. However, concomitantly to this shift, a decrease of the reflectivity amplitude is also expected as the electronic density, thus the Ga content, increases. This is not the case. Actually, for the 9% doped sample, the peak is rather small. This can be explained by the large chemical inhomogeneity of that sample reported previously. Indeed, among the sample, few nanocrystals are actually doped at 9%. Some are less doped whereas others have exceeded the solubility limit. The latter do not contribute to the plasmon signal. Another hypothesis to explain our data could be intraband absorption. Since the nanocrystals have a significant free electron density, they can induce an intraband absorption in the conduction band. Assuming that each Ga dopant contributes to the electronic density by one electron, the expected order of magnitude of the latter would be about a few 10^{20} cm^{-3} (see table 1). For such a concentration, A. Germeau *et al.* [34] have shown that the intraband absorption is located at

approximately 5 μm and is not so much dependent on the concentration of the electron gas. We thus safely believe that our observations are the signature of a localized surface plasmon resonance (LSPR) induced by the Ga incorporation, even though a minor contribution of intraband absorption cannot completely be excluded in the 5 μm range.

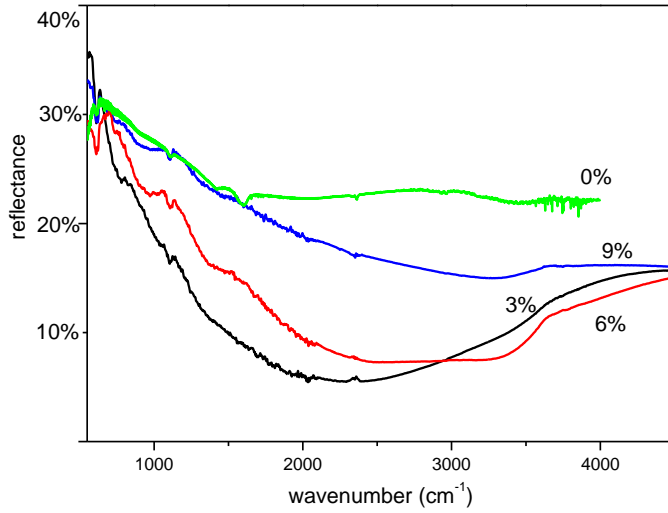


Figure 4: FTIR reflectance spectra of GZO nanoparticles films with different Ga content deposited on Si substrates. A slight contribution of the OH vibration modes at approximately 3400 cm^{-1} (3 μm) can be seen in the 6% sample spectrum.

We subsequently deduce the electron density corresponding to the observed peaks. Using the simple Drude's model, the frequency of the bulk plasmon resonance ω_p is related to the electron density n through:

$$\omega_p = \sqrt{\frac{ne^2}{\epsilon_0\epsilon_r m^*}} \quad (1)$$

Where e is the electron charge, m^* the effective mass of free electrons in ZnO (assuming it is not significantly perturbed by the high electron density value), ϵ_0 the permittivity of free space and ϵ_r the relative permittivity of ZnO. The surface plasmon induced in a collection of identical particles dispersed in a surrounding medium with a permittivity ϵ_m is:

$$\omega_{sp} = \sqrt{\frac{\omega_p^2}{\epsilon_\infty + 2\epsilon_m}} \quad (2)$$

Where ϵ_∞ is the high frequency permittivity of GZO (we approximate it with the value of 3.7 reported for ZnO [35]).

The estimation of ϵ_m is not straightforward. For particles diluted in a dielectric medium, the Maxwell-Garnett model is well adapted. However, this does not correspond to the case of our samples where nanoparticles are connected and touch each other forming a random network with 70% porosity (3D percolation limit). We have thus preferred the Bruggeman model to describe our samples. The medium surrounding a given nanocrystal is treated as a mixture of 30% GZO and 70% of air. Using this treatment, we extract the electron density values reported in table 1. The free carrier concentration varies from $1.8 \times 10^{20} \text{ cm}^{-3}$ to $4.1 \times 10^{20} \text{ cm}^{-3}$ which corresponds to 700 up to 1600 electrons per particle respectively. Mendelsberg *et al.* [23] have shown that equation 2 actually induces an inherent error in the determination of ω_p from ω_{sp} for degenerate semiconductor nanoparticles. Consequently, the values reported here must be considered as approximations (overestimations) of the real ones. Ga is a shallow donor when properly introduced in ZnO with an activation energy of about 16 meV, much lower than the thermal activation energy at room temperature. A striking fact is the difference between the Ga concentration and the actual free electron density. The two quantities differ by a factor of 2, meaning that at best (keeping in that the carrier concentration is overestimated), only 1/2 of the Ga atoms introduced effectively contribute to the free electron gas. The value seems low but it is in accordance with most of the reported values and in particular those for Al doped ZnO particles or ITO particles [22,24]. Moreover, our spectra present an asymmetrical line shape as reported by Milliron *et al.* [24]. Following the results from Milliron and co-workers, the last two observations can be consistently explained by the random distribution of the dopants among the nanocrystals.

We can further propose that a large fraction of the electrons provided by the Ga atoms are trapped at the numerous defects, such as twin boundaries, dislocations and dangling bonds possibly located at the interfaces of the nanocrystals. Recalling that unprotected surfaces of ZnO are highly sensitive

to air moisture and contamination and that this sensitivity leads to the presence of a depletion region underneath the surface, we can understand why so many electrons are lost for the LSPR. To sum it up, there may be two causes for the low activation of dopants: the first one is the incorporation of Ga atoms in inefficient sites, the second one is the trapping of free electrons at defects at the surface or interfaces. These two causes are not independent since inefficient sites for Ga atoms can be defects at the surface of the nanocrystals. If we stick to the simple model of the surface depletion region commonly evoked for ZnO nanoparticles, considering an activation of 1/2 of the Ga dopants and assuming the dopants are homogeneously distributed within each particle (as explained above) this leads to define a 2 nm “dead layer” below the surface of our 20 nm nanocrystals where the dopants are not activated.

Nanoparticles embedded in matrix

In order to investigate the parameters ruling the LSPR and its damping, related to the full-width-at-half-maximum (FWHM), we have embedded the 3% GZO nanocrystals in an Al₂O₃ matrix. The alumina matrix has been deposited using an electron gun for sublimation concomitantly to the nanocrystal deposition at much higher rate to ensure the nanocrystals are isolated. Hence they do not undergo OA. Contrary to the case of a nanoparticle assembled film, their size dispersion is known and is identical to the one of the isolated particles of fig. 1b, i.e. 5.6 ± 0.3 nm. The corresponding reflectance spectrum is presented on fig. 5 along with that of the same nanocrystals not embedded in the matrix. We first observe that the LSPR is red-shifted to 2100 cm^{-1} ($4.7 \text{ }\mu\text{m}$) when the nanocrystals are embedded in the alumina matrix. This is in agreement with equation (2) where ϵ_m is now the permittivity of the effective medium consisting of the alumina matrix and the GZO the particles. In this case, the Maxwell-Garnett model is adapted and ϵ_m is 2.5, thus larger than that deduced in the case of a porous GZO nanoparticle film. This further goes to show that we are dealing with LSPR. However, the red-shift might also result from a decrease of the free electron density (see eq. 1). This hypothesis is not likely since in this case the GZO nanocrystals are isolated and fully

passivated by the surrounding alumina matrix. We can thus expect the number of surface traps and interface defects to be reduced. This is confirmed by applying Drude's model to the GZO nanoparticles embedded in the alumina matrix. We get an estimated free electron density of $1.14 \times 10^{20} \text{ cm}^{-3}$, slightly larger than in the case of the particle assembled film. The fraction of activated Ga atoms is here 0.34, instead of 0.3. The crystalline disorder is reduced whereas the chemical disorder (inhomogeneity of the Ga atoms), which is mainly controlled by the synthesis conditions, is not affected.

The last observation that can be made concerns the FWHM, thus the LSPR damping. When the nanocrystals do not interact through OA and are isolated, the FWHM is reduced from 2331 cm^{-1} to 1140 cm^{-1} . Complementarily to the results of Milliron *et al.* [24] stating the FWHM is ruled by the dopant segregation among the particles, our results show that the LSPR damping is also influenced by the organization of the nanocrystals. When the particles are connected via OA, with twin boundaries, dislocations, possibly strain at the particle interfaces, the disorder is increased, the mean free path of the electrons is decreased and leads to an increased damping.

Besides, a recent work [36] on gold nanoparticles has shown that interactions between particles broaden the plasmon resonance. Either the capacitive coupling between LSPR of metal nanoparticles separated by a few nm or the delocalization of LSPR over fused metal nanoparticles lead to a spectral distribution of the LSPR. When a statistical variation of either the separating distance or of the number of fused metallic nanoparticles is present, the addition of the stochastically shifted LSPR leads to a broadened plasmon resonance. The FWHM of the plasmon resonance is thus not directly linked to the plasmon damping here. In our case the OA plays the same role as the fusion of the particles in the work of Dujardin *et al.* [36]. By attaching via epitaxy the initial nanoparticles, the OA process leads to a delocalization of the LSPR over several nanoparticles (the number of epitaxially attached nanoparticles varying among the sample), resulting eventually in a broad plasmon spectrum consisting of the sum of several shifted LSPR. When the OA is forbidden by embedding the particles in the matrix, the delocalization is not possible and hence the FWHM of the plasmon resonance is

reduced. This statement may also explain the general broadening of the LSPR observed in most of the studies devoted to particle assembled films.

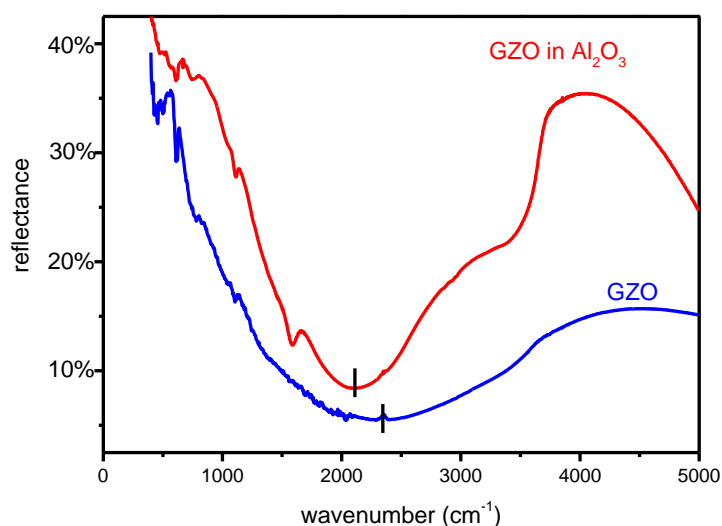


Figure 5: reflectance of 3% doped GZO nanocrystals assembling as a film or embedded in a Al_2O_3 matrix. The spectra are vertically shifted for the sake of clarity. The LSPR of the isolated GZO nanocrystals is red-shifted, in accordance with Drude's model and the FWHM is reduced. The small contribution around 3400 cm^{-1} is due to OH vibration mode.

Conclusions

We have synthesized by adiabatic expansion Ga doped ZnO nanoparticles in the gas phase. The resulting clusters are crystallized and self-organize during deposition through oriented attachment, leading to nanocrystals of 20 nm of mean size. The incorporation of Ga up to 6% is efficient and homogeneous whereas for 9% Ga concentration, the Ga atoms are inhomogeneously distributed from particle to particle. The chemical analysis reveals that the Ga atoms are linked to O atoms and that 1/2 of them do not efficiently contribute to the LSPR. Nevertheless, the free electron

concentration can be tuned from $1.8 \cdot 10^{20} \text{ cm}^{-3}$ to $4.1 \cdot 10^{20} \text{ cm}^{-3}$. Accordingly, the LSPR is tuned from 4 μm to 3 μm . The LSPR are characterized by large damping, as reported for other metal oxide plasmonic nanocrystals. The damping is reduced when the GZO nanocrystals are isolated in an alumina matrix, thus forbidding the oriented attachment to occur. Complementarily to recent results from the literature stating the damping is ruled by the dopant segregation among the particles, our results show that the LSPR damping is also influenced by the organization of the nanocrystals. Of prime importance is the surface and interface state of the plasmonic oxide nanoparticles in limiting the activation of the dopants.

Acknowledgements:

The authors acknowledge the PLYRA (Plateforme Lyonnaise de Recherche sur les Agrégats <http://www-lpmcn.univ-lyon1.fr/plyra/>) platform for access to the nanoparticle generators. Thanks are due to the CLYM (Centre LYonnais de Microscopie <http://www.clym.fr>) for the access to the microscope JEOL 2010F and the IPNL (Institut de Physique Nucléaire de Lyon) for access to the Van de Graaff accelerator for RBS measurements.

-
- ¹ X. Liu and M.T. Swihart, *Chem. Soc. Rev.* 2014, **43**, 3908-3920
- ² A. Comin and L. Manna, *Chem. Soc. Rev.* 2014, **43**, 3957-3975
- ³ G. V. Naik, J. Kim, A. Boltasseva, *Optical Materials Express*, 2011, **1**, 1090
- ⁴ A. K. Pradhan, R. M. Mundle, K. Santiago, J.R. Skuza, B. Xiao, K. D. Song, M. Bahoura, R. Cheaito, P. E. Hopkins, *Scientific Reports*, 2014, **4**, 6415
- ⁵ S. Kalusniak, S. Sadofev, F. Henneberger, *Phys. Rev. Lett.*, 2014, **112**, 137401
- ⁶ G. V Naik, J. Liu, A. V Kildishev, V. M. Shalaev, A. Boltasseva, *Proceedings of National Academy of Sciences*, 2012, **109**, 8834-8838
- ⁷ G. V Naik, J. Liu, A. V Kildishev, V. M. Shalaev, A. Boltasseva, *Proceedings of National Academy of Sciences*, 2012, **109**, 8834-8838
- ⁸ A. M. Schimpf, C. E. Gunthardt, J. D. Rinehart, J. M. Mayer, D. R. Gamelin, *J. Am. Chem. Soc.*, 2013, **135**, 16569-16577
- ⁹ J. A. Faucheaux and P. K. Jain, *J. Phys. Chem. Lett.* 2014, **4**, 3024-3030
- ¹⁰ F. Scotognella, G. Della Valle, A. R. S. Kandada, D. Dorfs, M. Zavelani-Rossi, M. Conforti, K. Miszta, A. Comin, K. Korobchevskaya, G. Lanzani, L. Manna, F. Tassone, *Nano Lett.* 2011, **11**, 4711-4717
- ¹¹ J. A. Faucheaux, A. L. D. Stanton, P. K. Jain, *J. Phys. Chem. Lett.*, 2014, **5**, 976-985
- ¹² S. B. Lounis, E. L. Runnerstrom, A. Llordés, D. J. Milliron, *J. Phys. Chem. Lett.*, 2014, **5**, 1564-1574
- ¹³ E. Della Gaspera, A. S. R. Chesman, J. van Embden, J. J. Jasieniak, *ACS Nano*, 2014, **8**, 9154-9163
- ¹⁴ S. Ghosh, M. Saha, S. Kumar De, *Nanoscale*, 2014, **6**, 7039-7051
- ¹⁵ E. Della Gaspera, M. Bersani, M. Cittadini, M. Guglielmi, D.R. Pagani, R. Noriega, S. Mehra, A. Salleo, A. Martucci, *J. Am. Chem. Soc.* 2013, **135**, 3439-3448
- ¹⁶ I. Kriegel, C. Jiang, J. Rodríguez-Fernández, R. D. Schaller, D. V. Talapin, E. da Como, J. Feldmann *J. Am. Chem. Soc.* 2012, **134**, 1583-1590
- ¹⁷ I. Kriegel, J. Rodríguez-Fernández, C. Jiang, R. Schaller, E. da Como, D. V. Talapin, J. Feldmann, *Selected Lectures Presented at Symposium on Ultrafast Dynamics of the 7th International Series in Optics and Photonics*, 2014, **8**, 272-291
- ¹⁸ P. K. Jain, K. Manthiram, J. Engel, S. L. White, J. A. Faucheaux, and A. P. Alivisatos, *Angew. Chem. Int. Ed.* 2013, **52**, 13671-13675
- ¹⁹ S. Kalusniak, S. Sadofev, F. Henneberger, *Proc. SPIE* 2014, doi:10.1117/12.2042235
- ²⁰ G. V. Naik, V.M. Shalaev, A. Boltasseva, *Adv. Mater.*, 2013, **25**, 3264-3294
- ²¹ J. Kim, G. V. Naik, A. V. Gavrilenko, K. Dondapati, V. I. Gavrilenko, S. M. Prokes, O. J. Glembocklti, V. M. Shalaev, A. Boltasseva, *Phys. Rev. X*, 2013, **3**, 041037
- ²² R. Buonsanti, A. Llordés, S. Aloni, B. A. Helms, D. J. Milliron, *Nano Letters*, 2011, **11**, 4706
- ²³ R. J. Mendelsberg, G. Garcia, H. Li, L. Manna, D. J. Milliron, *J. Phys. Chem. C* 2012, **116**, 12226_12231
- ²⁴ S. D. Lounis, E. L. Runnerstrom, A. Bergerud, D. Nordlund, D. J. Milliron, *J. Am. Chem. Soc.*, 2014, **136**, 7110-7116
- ²⁵ D. Tainoff, B. Masenelli, O. Boisron, G. Guiraud, P. Melinon, *J. Phys. Chem. C*, 2008, **112**, 12623-12627
- ²⁶ D. Hapiuk, B. Masenelli, K. Masenelli-Varlot, D. Tainoff, O. Boisron, C. Albin, P. Melinon, *J. Phys. Chem. C*, 2013, **117**, 10220-10227
- ²⁷ W. Lv, W. He, X. Wang, Y. Niu, H. Cao, J. H. Dickerson, Z. Wang, *Nanoscale* 2014, **6**, 2531-2547
- ²⁸ D. J. Norris, A. L. Efros, S. C. Erwin, *Science* 2008, **319**, 1776-1779
- ²⁹ H. Serier, A. Demourgues, M. Gaudon, *Inorg. Chem.* 2010, **49**, 6853-6858
- ³⁰ M. Passlack et al. *J. Appl. Phys.* 1995, **77**, 686-693
- ³¹ G. Cossu, G.M. Ingo, G. Mattogno, G. Padeletti, G.M. Proietti, *Appl. Surf. Sci.* 1992, **56**, 81
- ³² V. Bhosle, A. Tiwari, J. Narayan, *J. Appl. Phys.* 2006, **100**, 033713
- ³³ C.D. Wagner, *Discuss. Faraday Soc.* 1975, **60**, 291
- ³⁴ A. Germeau, A. L. Roest, D. Vanmaekelbergh, G. Allan, C. Delerue, E.A. Meulenkaamp, *Phys. Rev. Lett.*, 2003, **90**, 097401
- ³⁵ N. Ashkenov, B.N. Mbenkum, C. Bundesmann, V. Riede, M. Lorentz, D. Spemann, *J. Appl. Phys.* 2003, **93**, 126-133
- ³⁶ A. Teulle, M. Bosman, C. Girard, K. L. Gurunatha, M. Li, S. Mann, E. Dujardin, *Nat. Materials*, 2015, **14**, 87-94